THE JOURNAL OF PHYSICAL CHEMISTRY C
A JOURNAL OF THE AMERICAN CHEMICAL SOCIETY

pubs.acs.org/JPCC

Article

Cations Mediate Lithium Polysulfide Adsorption in Metal−Organic Frameworks for Lithium−Sulfur Batteries

Roberto A. Jarrín, Kevin Bennett, V. Sara Thoi, and Brandon C. Bukowski*

Cite This: J. Phys. Chem. C 2023, 127, 21431−21439

Read Online

ACCESS | Metrics & More | Article Recommendations | Supporting Information

ABSTRACT: Lithium−sulfur (Li−S) batteries are one promising alternative to Li-ion batteries due to their higher theoretical specific capacity and energy density. However, several technical challenges such as polysulfide shuttling remain. As liquid polysulfide diffusion into the electrolyte causes a loss of capacity, different material classes have been explored to anchor lithium polysulfides and reduce the active material loss. The metal−organic framework (MOF) UiO-66 has been identified as one candidate material due to its porosity, high surface area, and zirconium oxide nodes that could anchor liquid polysulfides. MOFs also allow for postsynthetic modifications that can increase their adsorption specificity toward liquid polysulfides and reduce shuttling. In this work, we combined atomistic simulations and experimental characterization to probe the molecular interactions between lithium polysulfides and functionalized UiO-66 nodes. We explored how lithium polysulfides adsorb to open sites caused by missing linker defects as well as sites functionalized with alkali cations. Our results demonstrate that lithium polysulfides adsorb favorably to UiO-66 through Li−O electrostatic interactions. In addition, we found that nodes functionalized with alkali metals demonstrated stronger adsorption of long-chain lithium polysulfides (Li_2S_{4-8}) by facilitating charge transfer to the nodes. Experimental ultraviolet-visible and ^{7}Li NMR measurements on Zr polyoxometalates and UiO-66 provided further evidence that lithiation favors adsorption of long-chain polysulfides. Our findings indicate that UiO-66 functionalization plays an important role in polysulfide adsorption, which may have implications in controlling the shuttle effect. The fundamental insights into polysulfide adsorption shown here provide quantitative principles to design functionalized moieties and further inhibit polysulfide shuttling.

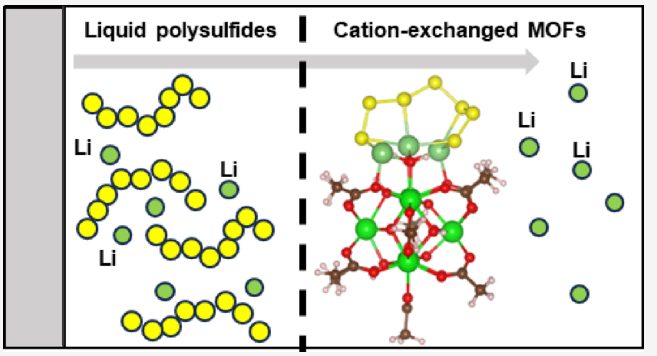

INTRODUCTION

The demand for improved energy storage technologies is increasing with the growth of the electric vehicle industry and decarbonization of the electric grid.[1] However, the current mass-produced lithium-ion batteries are limited by the energy density and specific capacity of their electrode materials. Common Li-ion batteries have energy densities around 250 Wh kg^{-1} and specific capacities around 200 mAh g^{-1}.[2] One alternative to current Li-ion batteries is lithium−sulfur (Li−S) batteries using S_8/Li_2S cathodes. Li−S batteries have been a subject of great interest due to their high theoretical energy density and specific capacity of 2500 Wh kg^{-1} and 1600 mAh g^{-1}, respectively.[3] The development of Li−S batteries currently faces several difficulties, including low conductivity of the electrode material, volume expansion during discharge, and the polysulfide shuttle effect.[4]

The shuttle effect in Li−S batteries arises from the stepwise reduction path of elemental sulfur (S_8) to lithium sulfide (Li_2S), where multiple different electrochemical reduction reactions occur at the cathode.[5] These include S_8 reduction to liquid polysulfides Li_2S_{4-8}, the reduction of Li_2S_4 to insoluble Li_2S_2, and the reduction of Li_2S_2 to Li_2S.[6] Liquid lithium polysulfide intermediates are highly soluble in ether electrolytes, allowing for diffusion from the cathode to the anode. This loss of active material leads to self-discharge, low cycling stability, and large overpotentials.[7]

To hinder the shuttle effect by way of restricting liquid lithium polysulfide diffusion via cathode coatings, a range of 2D and 3D materials have been studied for applications in Li−S batteries including polymers,[8−10] carbons,[11−13] Cu-BHT,[14,15] and metal−organic frameworks (MOFs) such as UiO-66 and MOF-808.[16−18] MOFs are promising materials for Li−S batteries as their high porosity and high surface area can permit ion diffusion while containing a large number of adsorption sites.[19−23] We have previously shown that increasing the number of missing linker defects and adding

Received: August 16, 2023
Revised: October 2, 2023
Published: October 19, 2023

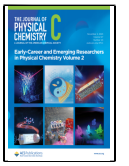

−OH and $-OH_2$ capping agents can further improve battery performance.[16,24,25] These missing linker defects expose polar oxygen sites that have been previously shown to effectively anchor lithium polysulfides by way of Li−O electrostatic interactions.[26,27] Functionalizing these MOFs has also been shown to further improve performance. One such modification is the replacement of node-bound protons with lithium, where modifying UiO-66 cathodes with both missing linker defects and lithiated sites was found to increase the cycling stability of Li−S cells relative to nonfunctionalized materials.[24]

UiO-66 comprises zirconium nodes $[Zr_6O_4(OH)_4]^{12+}$ with 12 linking sites, bridged by 1,4-benzenedicarboxylic acid (BDC) linkers. UiO-66 contains a smaller tetrahedral cage of 7.5 Å and a larger octahedral cage of 12 Å as well as a pore size of 6 Å. UiO-66 is characterized by its high porosity and surface area, theoretically reaching 0.77 $cm^3\ g^{-1}$ and 1160 $m^2\ g^{-1}$, respectively.[28] These textural properties permit Li^+ diffusion through many adsorption sites and open the possibility for further functionalization strategies.

Here, we performed atomistic simulations along with experimental ultraviolet-visible (UV−vis) and ^{7}Li NMR to probe the underlying chemistry behind polysulfide adsorption at defected MOF nodes. While the effect of UiO-66 films on cell capacity has been demonstrated, the molecular level interactions between lithium polysulfides and UiO-66 have not yet been explored. In this paper, we develop a molecular level understanding of the adsorption of lithium polysulfide to UiO-66 open sites driven by electrostatic and steric interactions. We performed density functional theory calculations to model lithium polysulfide adsorption as well as investigated how node functionalization using other alkali metals would affect adsorption. Experimental UV−vis and ^{7}Li NMR experiments on Zr polyoxometalates revealed that lithiation leads to changes in the speciation of adsorbed polysulfides.

METHODOLOGY

Density Functional Theory Calculations. We performed *ab initio* calculations with the ORCA density functional theory (DFT) package.[29−31] We used the M06 hybrid functional for electron−electron exchange and correlation interactions.[32] This functional was chosen as it has previously demonstrated accurate results for both polysulfides and metal−organic frameworks. For example, a DFT assessment of lithium polysulfide binding energies found that the M06 functional performed well with regard to both atomization energies and relative energies of Li_2S_n isomers.[33] M06 has also been shown to accurately model noncovalent interactions for adsorbates on metal−organic frameworks.[34−37]

The Def2-TZVP basis set was used in conjunction with the Def2/J and Def2-TZVP/C auxiliary basis sets.[38−41] RI and RIJCOSX approximations were both utilized to improve the computation time. van der Waals interactions were calculated with the D3ZERO atom-pairwise dispersion correction with the zero-damping scheme.[42] Geometry optimizations were performed with a convergence limitation of convergence 3.0×10^{-4} Ha $bohr^{-1}$.

MOF and Adsorbate Structures. We chose to represent a single node using nonperiodic DFT to reduce computation time and complexity, rather than simulate an entire periodic framework. This is justified by our focus on the initial adsorption process onto isolated nodes rather than polysulfide adsorption at saturation. The UiO-66 node is represented with a $[Zr_6O_4(OH)_4]^{12+}$ cation with the 12 linking sites represented with carboxylate CH_3COO^- groups. As this study focuses on adsorption to the node rather than to the linkers, these truncated linkers can adequately represent a BDC^{2-} linker. For the open node, an open or defect site is represented by a H_3OO^- group. A schematic of the node and missing linker defect is shown in Figure S1a. Open sites modified with alkali metals are produced by replacing a single hydrogen atom with an alkali metal atom in the most energetically favorable position discussed below.

We began by performing an initial geometry optimization using molecular dynamics simulations with xTB by Grimme.[43,44] xTB is a semiempirical tight-binding quantum mechanical method. It was used to perform molecular dynamics simulations and generate candidate geometries that were then optimized with DFT. These simulations used the GFN2-xTB[45] force field. Trials were performed at 298 K for 30 ps with a step of 2 fs and a hydrogen mass of 4 amu. Snapshot geometries obtained from MD were then relaxed with DFT.

Adsorption Thermodynamics. The adsorption energy was calculated according to eq 1.

$$\Delta E_{ads} = E_{PS,node} - E_{node} - E_{PS} \quad (1)$$

where $E_{PS,node}$ is the energy of lithium polysulfide adsorbed to the node, E_{node} is the energy of the node, and E_{PS} is the energy of the isolated charge neutral lithium polysulfide or other adsorbate. To better sample the possible node−polysulfide structures, we conducted geometry optimization trials combining the UiO-66 node and the lithium polysulfide, with the latter positioned near the open site. The positions of all carbon atoms were constrained during the optimization of the adsorbed polysulfide geometry to approximate the rigidity of the linkers in a periodic MOF structure. We additionally calculated Gibbs free energies in ORCA using the thermochemistry package, which used the harmonic oscillator approximation for adsorbed polysulfides. Gibbs free energy figures are presented in Figures S11 and S12.

Electronic Structure Calculations. Charge transfer analysis was conducted using Hirshfeld analysis,[46] which was calculated in ORCA. The charge to an atom or group of atoms during adsorption to the node can be expressed by the following:

$$\Delta Q_{atom(s)} = Q_{adsorbed} - Q_{free} \quad (2)$$

where $Q_{adsorbed}$ is the Hirshfeld charge of the atom(s), while in the adsorbate−node complex, and Q_{free} is the Hirshfeld charge of the atom(s) in the free or gaseous state.

RESULTS AND DISCUSSION

Node Modifications at Defect Sites. We introduced capping agents, one −OH group and one $-OH_2$ group, to replace the missing linker defects present in the material and generate an "open site". The open site structure is shown in Figure S1b. All lithium polysulfide adsorption geometries that we considered occur at the open site. In addition to the −OH and $-OH_2$ capping agents, the open site includes two Zr atoms, one μ_3-OH group and one μ_3-O group. The UiO-66 node with one open site was modified to produce a cation site by replacing one hydrogen atom with an alkali cation. We tested multiple cation adsorption sites to find the most energetically favorable adsorption configuration. The μ_3-OH hydrogen and $-OH_2$ hydrogen atoms both proved relevant as sites for modifications with the alkali metal, while the −OH

https://doi.org/10.1021/acs.jpcc.3c05539
J. Phys. Chem. C 2023, 127, 21431−21439

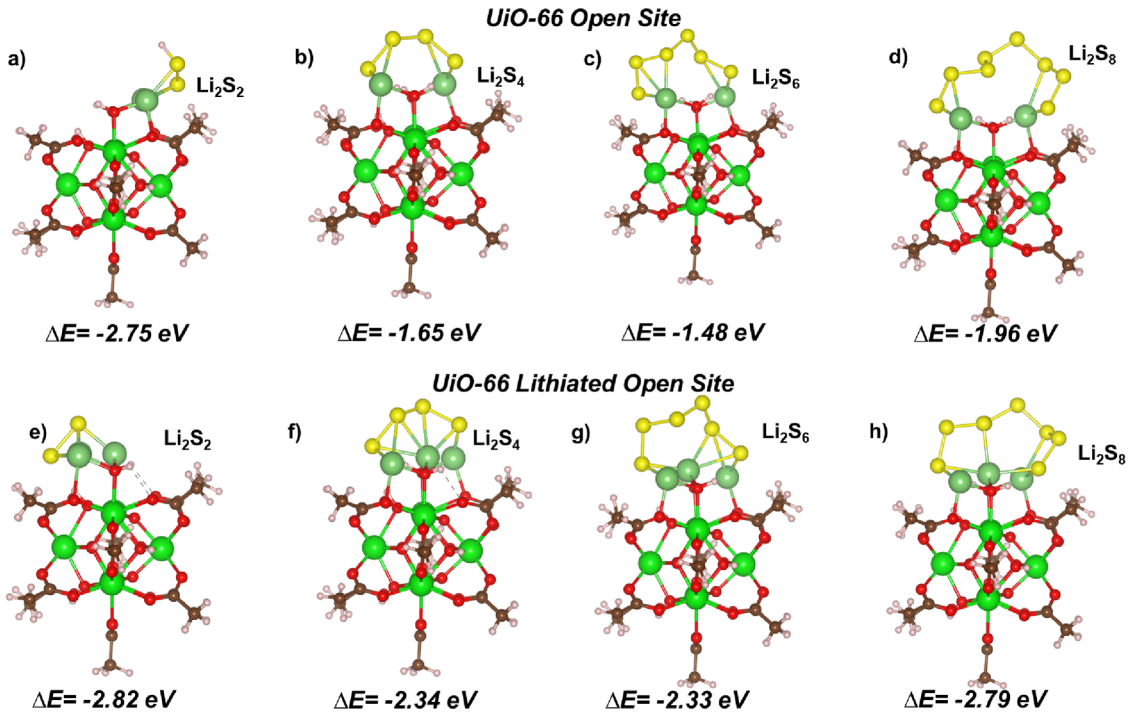

Figure 1. (a−h) Adsorption structures for Li_2S_{2n} on open sites and lithiated open sites at 298.15 K. Red (O), brown (C), gray (H), lime green (Zr), yellow (S), and green (Li).

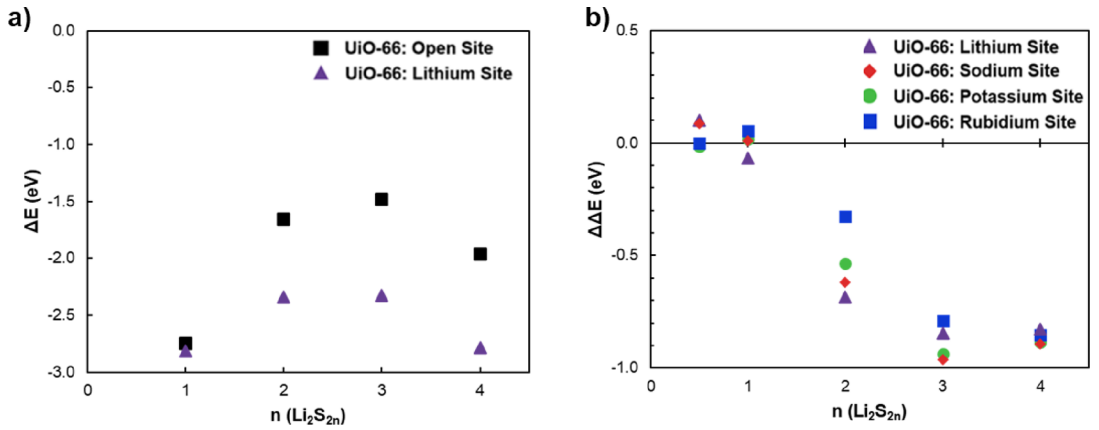

Figure 2. (a) Adsorption energy of lithium polysulfides to open sites and lithiated sites. (b) Differential adsorption energy of lithium polysulfides for cation-exchanged sites compared with open sites.

hydrogen was not. For all four alkali metal modifications tested, the alkali metal could adsorb at either the μ_3-OH or the $-OH_2$ position depending on lithium polysulfide size. The alkali metal was found to be the most energetically favorable in the $-OH_2$ position for the three smallest cations (Li, Na, and K), while Rb was more energetically favorable in the μ_3-OH position.

The free energy change of the alkali metal shift from the μ_3-OH position to the $-OH_2$ position increased with the cation size (Li: −0.44 eV, Na: −0.24 eV, K: −0.06 eV, Rb: +0.18 eV). This trend is likely due to strong Coulombic interactions between metals with larger radii and additional oxygen atoms when exchanged at the μ_3-OH position. In the $-OH_2$ position, all alkali metals are restricted to bonding with O_{-OH} and O_{-OH2} regardless of their ionic radius. A second contributor to the observed trend is the steric repulsion between the O_{-OH} and the O_{-OH2} at the open site when the alkali metal is in the $-OH_2$ position. The separation of these two oxygens is shown to increase with the period and ionic radius of alkali metal (H: 2.62 Å, Li: 3.50 Å, Na: 3.62 Å, K: 3.81 Å, Rb: 4.49 Å). The structures for the different cation-exchanged sites are shown in Figure S2.

Lithium Polysulfide Adsorption to the Open Site. Lithium polysulfides (Li_2S_{2n}, n = 1−4) were optimized in the gas phase and used as reference states to find the geometry and adsorption energy of lithium polysulfides at the UiO-66 open site. The adsorbed polysulfides on the open sites and lithium-exchanged sites are shown in Figure 1. Lithium atoms originating from the exchanged site will be denoted as Li_{node} compared to Li originating from the polysulfide denoted as Li_{PS}. The adsorption geometry of Li_2S_2 to the open site (Figure 1a) shows Li_2S_2 adsorbing to the μ_3-O side of the open site. The adsorption favorability is largely driven by Li−O electrostatic interactions. In addition, we see that the hydrogen

https://doi.org/10.1021/acs.jpcc.3c05539
J. Phys. Chem. C 2023, 127, 21431−21439

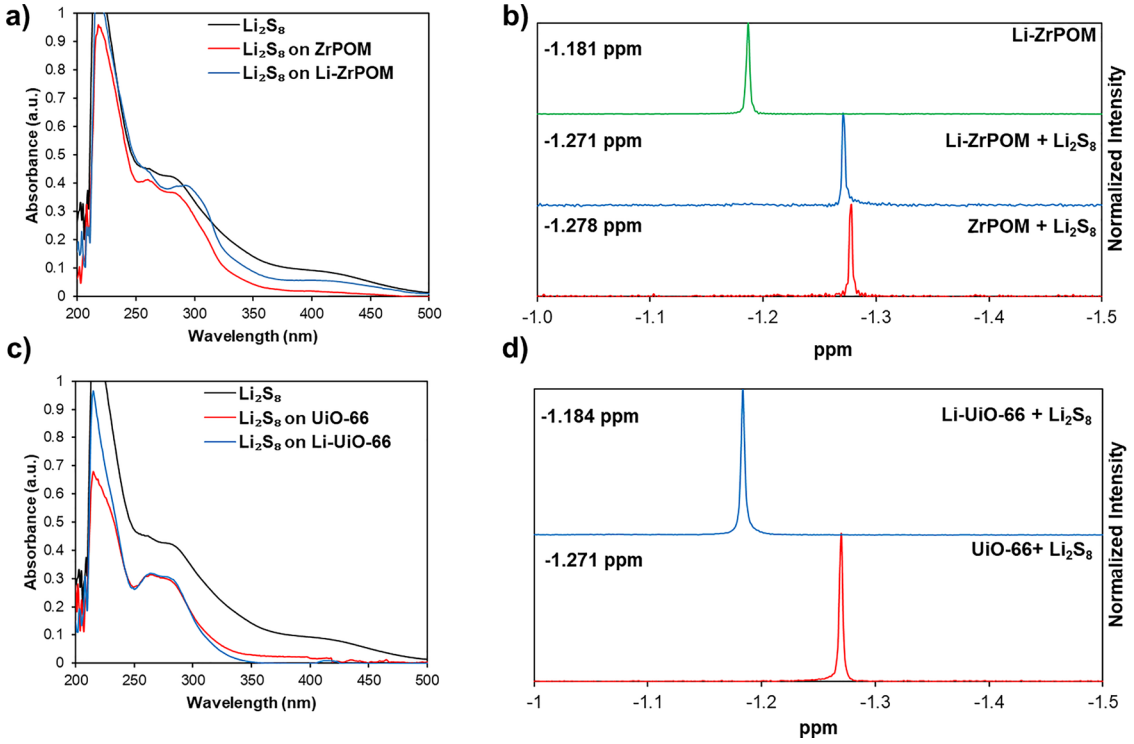

Figure 3. (a) UV−vis spectra of a Li_2S_8 solution (black) and a Li_2S_8 solution after the addition of ZrPOM (red) and Li-ZrPOM (blue). (b) ^{7}Li NMR spectra of ZrPOM (red) and Li-ZrPOM (blue) after soaking in Li_2S_8 and Li-ZrPOM before soaking (green). (c) UV−vis spectra of a Li_2S_8 solution (black) and Li_2S_8 solution after the addition of UiO-66 (red) and Li-UiO-66 (blue). (d) ^{7}Li NMR spectra of extracted lithium polysulfides from soaked UiO-66 (red) and Li-UiO-66 (blue). Absorbance solutions are in 1:1 DOL:DME, and NMR solutions are in DMSO-d_6. All NMR ppm shifts are referenced to LiCl in D_2O.

closest to H_{-OH2} has been replaced by Li. We observed this to occur spontaneously during geometry optimizations and verified by multiple initial conditions that this configuration was favorable. Adsorption of the three liquid polysulfides, Li_2S_4, Li_2S_6, and Li_2S_8, is driven by Li−O electrostatic interactions, and lithium replacement was found to be unfavorable (Figure 1b−d). The adsorbed Li ion on the μ_3-OH site interacts through Coulombic interactions with O−OH_2 and one OCH_3COO^-, and the Li on the μ_3-O interacts with O−OH and one OCH_3COO^-. Due to this diagonal configuration, the lithium atoms are further separated compared to the gas phase geometry as illustrated in Figure 1d where the Li−Li distance for adsorbed Li_2S_8 increases from 2.77 to 5.22 Å.

The sulfur ring remains largely unchanged during adsorption, where the main geometric difference between the gas phase and the adsorbed polysulfides is an increase in the separation between the two Li bonded sulfur. As both Li ions are further separated in the adsorbed geometry, both sulfurs bond with only one lithium, as opposed to bonding to both Li^+ ions at equal distances in the gas phase.

Lithium Polysulfide Adsorption to Lithium-Exchanged Sites. The adsorption of Li_2S_2 to the lithium site resulted in a geometry with notable differences as compared to adsorption to the open site, as shown in Figure 1e−h. Li_2S_2 adsorbs to the μ_3-O side of the open site, Li_{node} occupies the $-OH_2$ position, and there is no longer a hydrogen replacement from $-OH_2$. Despite the different adsorption geometries of Li_2S_2 to the open site and the lithium-exchanged site, the adsorption energy is slightly exergonic after the lithium functionalization ($\Delta\Delta E_{Li2S2}$ = +0.07 eV). The adsorption energies as a function of polysulfide length are shown in Figure 2a.

The adsorption geometries of the longer chain lithium polysulfides Li_2S_{4-8} to the Li site also show differences from the adsorption geometry to the open site. Both polysulfide Li atoms retain the same position relative to the open site. In all three adsorption geometries, Li_{node} occupies the $-OH_2$ position, and multiple polysulfide chain sulfur atoms interact with Li_{node}. The total number of Li−S interactions within 3 Å is greater in the adsorbed geometry to the Li site than in the open site. These new interactions and charge transfer between Li_{node} are additional effects that drive polysulfide adsorption to the Li node.

The adsorption energies of Li_2S_{4-8} are significantly affected by lithium functionalization. These polysulfides adsorb more favorably to the Li-modified site (Li_2S_4: $\Delta\Delta E$ = −0.68 eV, Li_2S_6: $\Delta\Delta E$ = −0.84 eV, Li_2S_8: $\Delta\Delta E$ = −0.83 eV). This improvement in adsorption favorability of liquid lithium polysulfides after lithium functionalization of the open site suggests that lithium-ion exchange can improve the lithium polysulfide anchoring capabilities of UiO-66 nodes with missing linker defects.

Experimental Characterization of Adsorbed Polysulfides. We synthesized Zr polyoxometallates ($Zr_6O_4(OH)_4L_{12}$, where L = propanoate)[47] as models of the Zr nodes to characterize polysulfide speciation on lithiated nodes. An HCl activation process similar to previously reported MOF procedures was used to remove the propanoate ligands and mimic the calculated node models. The HCl-activated Zr polyoxometalates are herein denoted as ZrPOM. We subsequently deprotonated and lithiated with triethylamine

https://doi.org/10.1021/acs.jpcc.3c05539
J. Phys. Chem. C 2023, 127, 21431−21439

and $LiNO_3$.[24] The lithiated Zr polyoxometallates were denoted as Li-ZrPOM. More details on the synthesis and characterization of Zr polyoxometallates can be found in the Supporting Information (Figures S3 and S4).

We performed polysulfide adsorption studies by soaking the Zr polyoxometallates in Li_2S_8 in 1:1 dimethoxymethane:dioxalane (1:1 DOL:DME) solutions. Lithium polysulfide solutions contain an equilibrium of polysulfide chains of various lengths, which can be evaluated by UV−vis absorbance spectroscopy. Peaks around 280, 315, and 410 nm are attributed to various chain lengths of S_x^{2-} (x = 8, 6, and 4, respectively) as reported in literature.[48,49] In Figure 3a, the absorbance profile of the resulting supernatant is notably different for ZrPOM compared to Li-ZrPOM. The red-shifted absorbance profile of Li-ZrPOM indicates the presence of shorter-chained lithium polysulfides in the supernatant compared to those in the ZrPOM supernatant. This observation is corroborated by ^{7}Li NMR spectroscopy of isolated ZrPOM and Li-ZrPOM before and after soaking in Li_2S_8 solutions (Figure 3b). After reuptake of the Li-ZrPOM and soaked Zr polyoxometalates in DMSO-d_6, we observe that the resulting ^{7}Li NMR spectra of residual lithium polysulfides exhibit single narrow and symmetrical peaks, which points to high lithium mobility and rapid lithium exchange in solution. Loss of a clearly defined peak for the untreated Li-ZrPOM in the spectra of soaked Zr polyoxometalates shows that lithium is exchanged not only across polysulfide species but also with dissolved Li-ZrPOMs. In addition, the ^{7}Li NMR signal of Li_2S_8-soaked Li-ZrPOM is downfield relative to that of the Li_2S_8-soaked ZrPOM, suggesting a small shift in equilibrium toward shorter-chained lithium polysulfides as short polysulfide chains decreases the relative shielding of Li^+ (Figure S5).[50]

We also experimentally compared polysulfide adsorption in nonlithiated and lithiated UiO-66 (denoted as UiO-66 and Li-UiO-66, respectively) to interrogate the influence of pore confinement on polysulfide adsorption, which is not captured in our computational model. Interestingly, both MOFs adsorbed lithium polysulfides nearly equally, likely because the pores play a dominant role in the physical encapsulation of lithium polysulfides (Figure 3c). A near complete loss of the S_4^{2-} peak at 410 nm in the supernatant solution is attributed to the enhanced pore penetration of the smaller chain-length polysulfides in the framework. We next conducted ^{7}Li NMR spectroscopy to track polysulfide speciation. The MOF powders soaked in Li_2S_8 solutions were isolated and resuspended in DMSO-d_6 to extract the trapped polysulfides. The subsequent ^{7}Li NMR spectra showed that the chemical shift of Li-UiO-66 is downfield compared to that of UiO-66 (Figure 3d), which suggests that the extracted lithium polysulfide is shifted to the short-chained species in Li-UiO-66. This result is consistent with our computational analysis that Li_2S_8 is held more tightly to lithiated nodes than Li_2S_4 and further indicates that our polyoxometalate models provide insight into adsorption onto MOF nodes. In addition, the rapid lithium exchange observed in the ^{7}Li NMR spectra corroborates the finding that Li_{node} (Li belonging to the lithiated site) participates in adsorption and is likely solvated.

Lithium Polysulfide Adsorption to Alkali Cation-Exchanged Sites. We investigated the role of different exchange cations in polysulfide adsorption. Lithium polysulfide adsorption to the larger alkali cation sites followed a similar pattern to adsorption to the lithium exchange sites. Full adsorption geometries of Li_2S_{2n} on all alkali metal-modified sites can be found in Figures S6−S10. Similar to the lithium-exchanged site, adsorption energies of Li_2S_{4-8} to the heavier alkali metal sites are more energetically favorable than those of adsorption to the open site. The polysulfide adsorption energy to each cation-exchanged site is shown in Table 1. Differential changes in polysulfide adsorption on alkali-exchanged sites relative to the open site are shown in Figure 2b as a function of the polysulfide size.

Table 1. Adsorption Energies of Lithium polysulfides to the Open Site and to Alkali Metal Functionalized Sites

	ΔE_{ads} (eV)				
n (Li_2S_{2n})	open	Li	Na	K	Rb
1	−2.75	−2.82	−2.74	−2.73	−2.70
2	−1.65	−2.34	−2.27	−2.19	−1.98
3	−1.48	−2.33	−2.45	−2.42	−2.27
4	−1.96	−2.79	−2.85	−2.85	−2.81

Adsorption Energy Decomposition. To relate the polysulfide adsorption energy to the alkali metal identity, we decomposed the adsorption energy into three components each associated with an energy contribution. These components are an alkali cation shift (ΔE_{shift}), the lithium polysulfide geometric deformation (ΔE_{deform}), and the intrinsic lithium polysulfide/open site interaction ($\Delta E_{interact}$). The full expression of the adsorption energy separated into individual components is given in eq 3:

$$\Delta E_{ads} = \Delta E_{shift} + \Delta E_{deform} + \Delta E_{interact} \quad (3)$$

The alkali metal shift involves the energy change of the cation exchanged at the node shifting between the μ_3-OH and $-OH_2$ positions upon adsorption. This value is always positive if a shift is present or zero if no shift during the adsorption process occurs. The deformation energy is defined as the change in energy of the polysulfide's most stable gas phase geometry to its adsorbed configuration. As this geometric deformation is defined relative to the gas phase configuration, this term is always positive. Finally, the interaction energy change includes all other energetic effects involving interactions between the polysulfide and the node. This energy is negative. In Figure 4a, we see a positive relationship when the interaction energy is plotted against the ionization energy of alkali metal. This shows that sites with heavier alkali metals with loosely held valence electrons lead to the most favorable interactions between the node and the polysulfide. As shown in Figure 4b, for any given polysulfide, the ionic radius of the alkali metal and the deformation energy are positively correlated. This trend shows that increases in the cation van der Waals volume lead to geometric deformation of the polysulfide and an associated increase in energy. This is the opposite trend compared to that for the interaction energy, which scales negatively with cation size. These competing relationships show that while larger alkali metals cause more unfavorable geometric deformations in the polysulfide, this is compensated for by a more favorable interaction between the polysulfide and the node.

Charge Transfer Analysis. To further explain why certain lithium polysulfides adsorbed more favorably than others and why alkali cation functionalization decreases polysulfide adsorption energy for liquid polysulfides, we analyzed electron density transfer and Hirshfeld partial charges of lithium polysulfide and open site atoms. Figure 5 shows electron

https://doi.org/10.1021/acs.jpcc.3c05539
J. Phys. Chem. C 2023, 127, 21431−21439

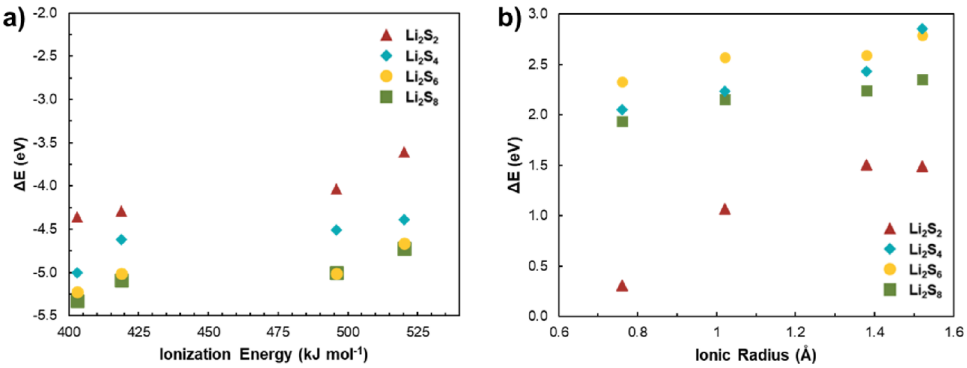

Figure 4. (a) Adsorption energy change of polysulfide geometric deformation during adsorption to cation-exchanged nodes against cation first ionization energy. (b) Adsorption energy change of lithium−polysulfide interaction energy during adsorption to cation-exchanged nodes against the cation ionic radius.

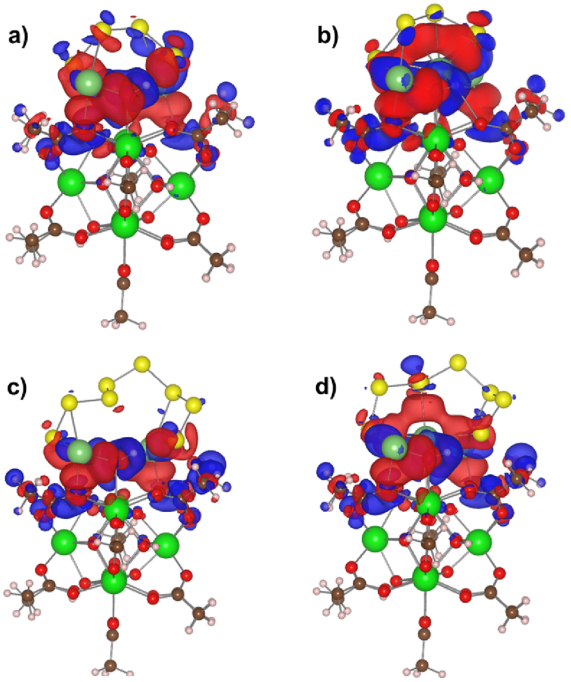

Figure 5. Electron density change isosurface plots (red: +0.0012 e^-, blue: −0.0012 e^-) for (a) Li_2S_4 adsorption to the open site, (b) Li_2S_4 adsorption to the Li site, (c) Li_2S_8 adsorption to the open site, and (d) Li_2S_8 adsorption to the Li site.

density transfer plots for Li_2S_4 and Li_2S_6 adsorption to the open site and Li site. These plots show transfer of electron density arising from the interactions between the lithium polysulfide and the UiO-66 node. Both plots show increased electron density around the Li atoms originating from the polysulfide and decreased density around O and H atoms in the node. The main difference between the two diagrams is the volume of increased electron density between Li_{node} and the sulfur ring that is present in Figure 5b,d but not in Figure 5a,c. This is visual evidence of sulfur rings promoting electron transfer from the node to M_{node}. This volume of increased electron density under the sulfur ring is only present when adsorbed to an alkali metal functionalized site.

We used charge analysis to show why Li_2S adsorbs more favorably than other lithium polysulfides. Hirshfeld charges are listed in Figure 5. Based on our charge analysis data, we distinguish two different sulfur atom types: α-sulfur is sulfur atoms that are nearest-neighbor to lithium, whereas β-sulfur is nearest-neighbor to other sulfur atoms. The average partial charge of lithium decreases from +0.40 to +0.27 e, and the α-sulfur partial charge increases from −0.81 to −0.36 e. As shown in Figures 6a,b, Li_2S has significantly more charge transfer than the other polysulfides. Li_2S_2, the next most favorably adsorbing lithium polysulfide, also has significant charge transfer. Lithium partial charges decrease from +0.40 to between +0.27 and +0.22 e when adsorbed. It should be noted that in Figure 6b, the average α-sulfur partial charge for Li_2S_2 adsorbed to the open site is larger than the partial charges adsorbed to the alkali metal sites. The difference in α-sulfur partial charges leads to Li_2S_2 adsorbing more favorably to the open site than to any alkali metal functionalized site. Figure 5c shows that β-sulfur has negligible charge transfer (on the order of 0.05 e), showing that charge transfer predominantly occurs proximal to lithium for all polysulfides.

The partial charge of cations exchanged on the node (Figure 6d) can explain the increased energetic favorability of liquid polysulfide adsorption to alkali metal sites compared with the open site. Without adsorbates, cation sites have a large positive partial charge, while the remainder of the node has a large negative partial charge. The largest changes in both partial charges occur during the adsorption of Li_2S_6 and Li_2S_8, both of which have large negative $\Delta\Delta E$ values (Table 1). This leads to the proposed mechanism by which alkali metal functionalization increases adsorption favorability of liquid polysulfides: long sulfur rings energetically stabilize the exchange alkali atoms upon adsorption by allowing electron transfer from the negatively charged node into the positively charged alkali metal. Longer sulfur chains permit the reorganization of charge at alkali exchange sites, which stabilizes the adsorption energy of the liquid polysulfides.

Electrolyte Adsorption. We calculated electrolyte adsorption energies to determine whether competitive adsorption would occur at open sites or cation-exchanged sites. A common electrolyte used in Li−S cells is 1 M LiTFSI in 1:1, v:v DOL/DME.[25] We calculated the adsorption energies of DOL, DME, and the $TFSI^-$ anions to the open site and the Li site and found that their adsorption free energies are weaker than those of all polysulfides by at least 0.64 eV for open sites and 0.94 eV for Li exchange sites. DOL, DME, and $TFSI^-$ adsorption energies are shown in Table S1. These data indicate that polysulfides preferentially adsorb to defect sites at the node compared to the electrolyte solution.

https://doi.org/10.1021/acs.jpcc.3c05539
J. Phys. Chem. C 2023, 127, 21431−21439

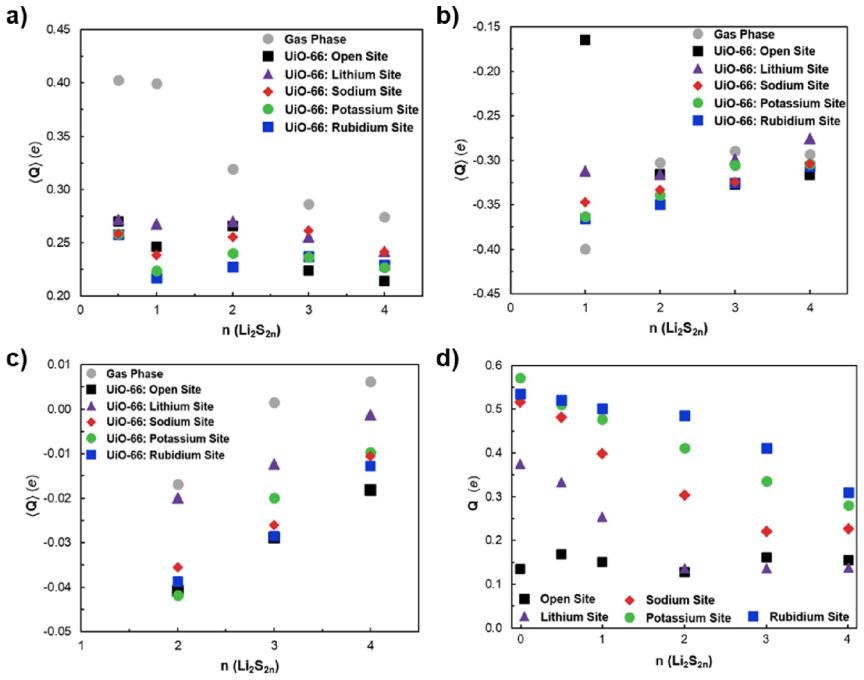

Figure 6. (a) Average Hirshfeld partial charges of Li atoms in lithium polysulfides in the gas phase calculation and adsorbed to the open site and alkali metal functionalized sites. Average Hirshfeld partial charges of (b) α-sulfur and (c) β-sulfur in the gas phase and adsorbed geometries. (d) Hirshfeld partial charges of the alkali metal originating from the node.

CONCLUSIONS

In this study, we demonstrated through *ab initio* simulations, UV−vis, and ^{7}Li NMR that missing linker defects in UiO-66 act as an anchor for adsorbing liquid lithium polysulfides. The open sites favorably adsorb lithium polysulfides through both Li−O and μ_3-OH electrostatic interactions with sulfur. We demonstrated that lithium polysulfides favorably adsorb to the open site, also driven by Li−O interactions, and that replacing hydrogen with alkali metal Li−Rb improves the adsorption energy of long-chain (Li_2S_{4-8}) lithium polysulfides. Alkali cations at the open site are energetically favorable, and we demonstrated that polysulfide adsorption to the alkali metal sites is dominated by alkali−sulfur charge interactions. These interactions lead to a transfer of electron density from the node to the sulfur ring, stabilizing charge on the node and increasing the energetic favorability of adsorption. The conclusions that lithiation stabilizes long-chain polysulfides were supported by UV−vis and ^{7}Li NMR adsorption experiments performed on Zr polyoxometalates and Zr-MOF, UiO-66. Finally, we demonstrated that common electrolytes do not compete with lithium polysulfides for adsorption to open and lithium functionalized sites.

These results show that defect engineering of MOFs with cation-exchange sites can anchor liquid polysulfides as a possible mechanism to prevent polysulfide shuttling in lithium−sulfur batteries, and that node functionalization provides an avenue for tuning electrostatic interactions, thereby modulating polysulfide adsorption.

ASSOCIATED CONTENT

Supporting Information

The Supporting Information is available free of charge at https://pubs.acs.org/doi/10.1021/acs.jpcc.3c05539.

Experimental procedures and simulation details (PDF)

ZIP folder containing XYZ files for the converged structures (ZIP)

AUTHOR INFORMATION

Corresponding Author

Brandon C. Bukowski − *Department of Chemical and Biomolecular Engineering, Johns Hopkins University, Baltimore, Maryland 21218, United States;* orcid.org/0000-0002-2626-8908; Email: bbukows1@jhu.edu

Authors

Roberto A. Jarrín − *Department of Chemical and Biomolecular Engineering, Johns Hopkins University, Baltimore, Maryland 21218, United States;* orcid.org/0009-0001-8631-9359

Kevin Bennett − *Department of Chemistry, Johns Hopkins University, Baltimore, Maryland 21218, United States*

V. Sara Thoi − *Department of Chemistry and Department of Materials Science and Engineering, Johns Hopkins University, Baltimore, Maryland 21218, United States;* orcid.org/0000-0003-0896-4077

Complete contact information is available at: https://pubs.acs.org/10.1021/acs.jpcc.3c05539

Notes

The authors declare no competing financial interest.

ACKNOWLEDGMENTS

R.A.J. and B.C.B. acknowledge the Advanced Research Computing at Hopkins (ARCH) Core Facility (rockfish.jhu.edu), which is supported by the National Science Foundation (NSF) grant number OAC1920103. K.B. and V.S.T. acknowledge the support of an NSF CAREER Award (DMR-1945114). We also thank the Ralph S. O'Connor Sustainable Energy Institute (ROSEI) at Johns Hopkins University for

support through the Light-Integrated Technology for Energy Storage (LITES) initiative.

REFERENCES

(1) Manzetti, S.; Mariasiu, F. Electric Vehicle Battery Technologies: From Present State to Future Systems. *Renewable Sustainable Energy Rev.* **2015**, *51*, 1004−1012.
(2) Kumar, R.; Liu, J.; Hwang, J.-Y.; Sun, Y.-K. Recent Research Trends in Li−S Batteries. *J. Mater. Chem. A* **2018**, *6* (25), 11582−11605.
(3) Li, F.; Zhao, J. Atomic Sulfur Anchored on Silicene, Phosphorene, and Borophene for Excellent Cycle Performance of Li−S Batteries. *ACS Appl. Mater. Interfaces* **2017**, *9* (49), 42836−42844.
(4) Ji, Z.; Han, B.; Li, Q.; Zhou, C.; Gao, Q.; Xia, K.; Wu, J. Anchoring Lithium polysulfides via Affinitive Interactions: Electrostatic Attraction, Hydrogen Bonding, or in Parallel? *J. Phys. Chem. C* **2015**, *119* (35), 20495−20502.
(5) Seh, Z. W.; Sun, Y.; Zhang, Q.; Cui, Y. Designing High-Energy Lithium−Sulfur Batteries. *Chem. Soc. Rev.* **2016**, *45* (20), 5605−5634.
(6) Ji, X.; Nazar, L. F. Advances in Li−S Batteries. *J. Mater. Chem.* **2010**, *20* (44), 9821.
(7) Mikhaylik, Y. V.; Akridge, J. R. polysulfide Shuttle Study in the Li/S Battery System. *J. Electrochem. Soc.* **2004**, *151* (11), A1969.
(8) Li, G.-C.; Li, G.-R.; Ye, S.-H.; Gao, X.-P. A Polyaniline-Coated Sulfur/Carbon Composite with an Enhanced High-Rate Capability as a Cathode Material for Lithium/Sulfur Batteries. *Adv. Energy Mater.* **2012**, *2* (10), 1238−1245.
(9) Yang, Y.; Yu, G.; Cha, J. J.; Wu, H.; Vosgueritchian, M.; Yao, Y.; Bao, Z.; Cui, Y. Improving the Performance of Lithium−Sulfur Batteries by Conductive Polymer Coating. *ACS Nano* **2011**, *5* (11), 9187−9193.
(10) Huang, J.-Q.; Zhang, Q.; Zhang, S.-M.; Liu, X.-F.; Zhu, W.; Qian, W.-Z.; Wei, F. Aligned Sulfur-Coated Carbon Nanotubes with a Polyethylene Glycol Barrier at One End for Use as a High Efficiency Sulfur Cathode. *Carbon* **2013**, *58*, 99−106.
(11) Liu, Y.; Li, G.; Chen, Z.; Peng, X. CNT-Threaded N-Doped Porous Carbon Film as Binder-Free Electrode for High-Capacity Supercapacitor and Li−S Battery. *J. Mater. Chem. A* **2017**, *5* (20), 9775−9784.
(12) Xiao, Z.; Yang, Z.; Wang, L.; Nie, H.; Zhong, M.; Lai, Q.; Xu, X.; Zhang, L.; Huang, S. A Lightweight TiO2/Graphene Interlayer, Applied as a Highly Effective polysulfide Absorbent for Fast, Long-Life Lithium−Sulfur Batteries. *Adv. Mater.* **2015**, *27* (18), 2891−2898.
(13) Zhou, G.; Paek, E.; Hwang, G. S.; Manthiram, A. Long-Life Li/Polysulphide Batteries with High Sulphur Loading Enabled by Lightweight Three-Dimensional Nitrogen/Sulphur-Codoped Graphene Sponge. *Nat. Commun.* **2015**, *6* (1), 7760.
(14) Li, F.; Zhang, X.; Liu, X.; Zhao, M. Novel Conductive Metal−Organic Framework for a High-Performance Lithium−Sulfur Battery Host: 2D Cu-Benzenehexathial (BHT). *ACS Appl. Mater. Interfaces* **2018**, *10* (17), 15012−15020.
(15) Bhauriyal, P.; Pathak, B. Superior Anchoring Effect of a Cu-Benzenehexathial MOF as an Aluminium−Sulfur Battery Cathode Host. *Mater. Adv.* **2020**, *1* (9), 3572−3581.
(16) Baumann, A. E.; Han, X.; Butala, M. M.; Thoi, V. S. Lithium Thiophosphate Functionalized Zirconium MOFs for Li−S Batteries with Enhanced Rate Capabilities. *J. Am. Chem. Soc.* **2019**, *141* (44), 17891−17899.
(17) Banerjee, S.; Han, X.; Siegler, M. A.; Miller, E. M.; Bedford, N. M.; Bukowski, B. C.; Thoi, V. S. Flexible 2D Boron Imidazolate Framework for polysulfide Adsorption in Lithium−Sulfur Batteries. *Chem. Mater.* **2022**, *34* (23), 10451−10458.
(18) Liu, B.; Baumann, A. E.; Butala, M. M.; Thoi, V. S. Phosphate-Functionalized Zirconium Metal−Organic Frameworks for Enhancing Lithium−Sulfur Battery Cycling. *Chem. - Eur. J.* **2023**, *29* (40), No. e202300821.
(19) Kondo, M.; Yoshitomi, T.; Matsuzaka, H.; Kitagawa, S.; Seki, K. Three-Dimensional Framework with Channeling Cavities for Small Molecules: [M2(4, 4′-Bpy)3(NO3)4]·xH2On (M = Co, Ni, Zn). *Angew. Chem., Int. Ed. Engl.* **1997**, *36* (16), 1725−1727.
(20) Yaghi, O. M.; Li, G. Mutually Interpenetrating Sheets and Channels in the Extended Structure of [Cu(4,4′-Bpy)Cl]. *Angew. Chem., Int. Ed. Engl.* **1995**, *34* (2), 207−209.
(21) Yaghi, O. M.; Li, G.; Li, H. Selective Binding and Removal of Guests in a Microporous Metal−Organic Framework. *Nature* **1995**, *378* (6558), 703−706.
(22) Valenzano, L.; Civalleri, B.; Chavan, S.; Palomino, G. T.; Areán, C. O.; Bordiga, S. Computational and Experimental Studies on the Adsorption of CO, N2, and CO2 on Mg-MOF-74. *J. Phys. Chem. C* **2010**, *114* (25), 11185−11191.
(23) Li, L.; Lin, R.-B.; Krishna, R.; Wang, X.; Li, B.; Wu, H.; Li, J.; Zhou, W.; Chen, B. Flexible−Robust Metal−Organic Framework for Efficient Removal of Propyne from Propylene. *J. Am. Chem. Soc.* **2017**, *139* (23), 7733−7736.
(24) Baumann, A. E.; Burns, D. A.; Díaz, J. C.; Thoi, V. S. lithiated Defect Sites in Zr Metal−Organic Framework for Enhanced Sulfur Utilization in Li−S Batteries. *ACS Appl. Mater. Interfaces* **2019**, *11* (2), 2159−2167.
(25) Baumann, A. E.; Aversa, G. E.; Roy, A.; Falk, M. L.; Bedford, N. M.; Thoi, V. S. Promoting Sulfur Adsorption Using Surface Cu Sites in Metal−Organic Frameworks for Lithium Sulfur Batteries. *J. Mater. Chem. A* **2018**, *6* (11), 4811−4821.
(26) Li, N.; Meng, Q.; Zhu, X.; Li, Z.; Ma, J.; Huang, C.; Song, J.; Fan, J. Lattice Constant-Dependent Anchoring Effect of MXenes for Lithium−Sulfur (Li−S) Batteries: A DFT Study. *Nanoscale* **2019**, *11* (17), 8485−8493.
(27) Wang, S.; Wang, Y.; Song, Y.; Jia, X.; Yang, J.; Li, Y.; Liao, J.; Song, H. Immobilizing polysulfide via Multiple Active Sites in W18O49 for Li-S Batteries by Oxygen Vacancy Engineering. *Energy Storage Mater.* **2021**, *43*, 422−429.
(28) Cavka, J. H.; Jakobsen, S.; Olsbye, U.; Guillou, N.; Lamberti, C.; Bordiga, S.; Lillerud, K. P. A New Zirconium Inorganic Building Brick Forming Metal Organic Frameworks with Exceptional Stability. *J. Am. Chem. Soc.* **2008**, *130* (42), 13850−13851.
(29) Neese, F. The ORCA Program System. *Wiley Interdiscip. Rev.: Comput. Mol. Sci.* **2012**, *2* (1), 73−78.
(30) Neese, F. Software Update: The ORCA Program System Version 4.0. *Wiley Interdiscip. Rev.: Comput. Mol. Sci.* **2018**, *8* (1), No. e1327.
(31) Lehtola, S.; Steigemann, C.; Oliveira, M. J. T.; Marques, M. A. L. Recent Developments in Libxc — A Comprehensive Library of Functionals for Density Functional Theory. *SoftwareX* **2018**, *7*, 1−5.
(32) Zhao, Y.; Truhlar, D. G. The M06 Suite of Density Functionals for Main Group Thermochemistry, Thermochemical Kinetics, Noncovalent Interactions, Excited States, and Transition Elements: Two New Functionals and Systematic Testing of Four M06-Class Functionals and 12 Other Functionals. *Theor. Chem. Acc.* **2008**, *120* (1−3), 215−241.
(33) He, Q.; Liao, X.; Xia, L.; Li, Z.; Wang, H.; Zhao, Y.; Truhlar, D. G. Accurate Binding Energies for Lithium polysulfides and Assessment of Density Functionals for Lithium−Sulfur Battery Research. *J. Phys. Chem. C* **2019**, *123* (34), 20737−20747.
(34) Bernales, V.; Ortuño, M. A.; Truhlar, D. G.; Cramer, C. J.; Gagliardi, L. Computational Design of Functionalized Metal−Organic Framework Nodes for Catalysis. *ACS Cent. Sci.* **2018**, *4* (1), 5−19.
(35) Xiao, D. J.; Bloch, E. D.; Mason, J. A.; Queen, W. L.; Hudson, M. R.; Planas, N.; Borycz, J.; Dzubak, A. L.; Verma, P.; Lee, K.; et al. Oxidation of Ethane to Ethanol by N2O in a Metal−Organic Framework with Coordinatively Unsaturated Iron(II) Sites. *Nat. Chem.* **2014**, *6* (7), 590−595.
(36) Verma, P.; Vogiatzis, K. D.; Planas, N.; Borycz, J.; Xiao, D. J.; Long, J. R.; Gagliardi, L.; Truhlar, D. G. Mechanism of Oxidation of Ethane to Ethanol at Iron(IV)−Oxo Sites in Magnesium-Diluted Fe_2(Dobdc). *J. Am. Chem. Soc.* **2015**, *137* (17), 5770−5781.

https://doi.org/10.1021/acs.jpcc.3c05539
J. Phys. Chem. C 2023, 127, 21431−21439

(37) Kumar, R. M.; Sundar, J. V.; Subramanian, V. Improving the Hydrogen Storage Capacity of Metal Organic Framework by Chemical Functionalization. *Int. J. Hydrogen Energy* **2012**, *37* (21), 16070−16077.
(38) Weigend, F.; Ahlrichs, R. Balanced Basis Sets of Split Valence, Triple Zeta Valence and Quadruple Zeta Valence Quality for H to Rn: Design and Assessment of Accuracy. *Phys. Chem. Chem. Phys.* **2005**, *7* (18), 3297.
(39) Weigend, F. Accurate Coulomb-Fitting Basis Sets for H to Rn. *Phys. Chem. Chem. Phys.* **2006**, *8* (9), 1057.
(40) Hellweg, A.; Hättig, C.; Höfener, S.; Klopper, W. Optimized Accurate Auxiliary Basis Sets for RI-MP2 and RI-CC2 Calculations for the Atoms Rb to Rn. *Theor. Chem. Acc.* **2007**, *117* (4), 587−597.
(41) Chmela, J.; Harding, M. E. Optimized Auxiliary Basis Sets for Density Fitted Post-Hartree−Fock Calculations of Lanthanide Containing Molecules. *Mol. Phys.* **2018**, *116* (12), 1523−1538.
(42) Grimme, S.; Antony, J.; Ehrlich, S.; Krieg, H. A Consistent and Accurate *Ab Initio* Parametrization of Density Functional Dispersion Correction (DFT-D) for the 94 Elements H-Pu. *J. Chem. Phys.* **2010**, *132* (15), 154104.
(43) Bannwarth, C.; Caldeweyher, E.; Ehlert, S.; Hansen, A.; Pracht, P.; Seibert, J.; Spicher, S.; Grimme, S. Extended Tight-Binding Quantum Chemistry Methods. *Wiley Interdiscip. Rev.: Comput. Mol. Sci.* **2021**, *11* (2), No. e1493.
(44) Grimme, S.; Bannwarth, C.; Shushkov, P. A Robust and Accurate Tight-Binding Quantum Chemical Method for Structures, Vibrational Frequencies, and Noncovalent Interactions of Large Molecular Systems Parametrized for All Spd-Block Elements (Z = 1−86). *J. Chem. Theory Comput.* **2017**, *13* (5), 1989−2009.
(45) Bannwarth, C.; Ehlert, S.; Grimme, S. GFN2-xTB—An Accurate and Broadly Parametrized Self-Consistent Tight-Binding Quantum Chemical Method with Multipole Electrostatics and Density-Dependent Dispersion Contributions. *J. Chem. Theory Comput.* **2019**, *15* (3), 1652−1671.
(46) Hirshfeld, F. L. Bonded-Atom Fragments for Describing Molecular Charge Densities. *Theor. Chim. Acta* **1977**, *44* (2), 129−138.
(47) Piszczek, P.; Radtke, A.; Grodzicki, A.; Wojtczak, A.; Chojnacki, J. The New Type of [Zr6(M3-O)4(M3-OH)4] Cluster Core: Crystal Structure and Spectral Characterization of [Zr6O4(OH)4(OOCR)-12] (R = But, C(CH3)2Et). *Polyhedron* **2007**, *26* (3), 679−685.
(48) Zou, Q.; Lu, Y.-C. Solvent-Dictated Lithium Sulfur Redox Reactions: An Operando UV−Vis Spectroscopic Study. *J. Phys. Chem. Lett.* **2016**, *7* (8), 1518−1525.
(49) He, Q.; Freiberg, A. T. S.; Patel, M. U. M.; Qian, S.; Gasteiger, H. A. Operando Identification of Liquid Intermediates in Lithium−Sulfur Batteries via Transmission UV−Vis Spectroscopy. *J. Electrochem. Soc.* **2020**, *167* (8), No. 080508.
(50) Dorai, A.; Kawamura, J.; Omata, T. Visualization of polysulfide Dissolution in Lithium-Sulfur Batteries Using in-Situ NMR Micro-imaging. *Electrochem. Commun.* **2022**, *141*, No. 107360.

https://doi.org/10.1021/acs.jpcc.3c05539
J. Phys. Chem. C 2023, 127, 21431−21439